



Available online at www.sciencedirect.com

ScienceDirect

Advances in Space Research 73 (2024) 1083-1091

ADVANCES IN SPACE RESEARCH (a COSPAR publication)

www.elsevier.com/locate/asr

High-altitude characterization of the Hunga pressure wave with cosmic rays by the HAWC observatory

Ruben Alfaro^a, César Alvarez^b, Juan Carlos Arteaga-Velázquez^c, Arun Babu Kollamparambil Paul ac, Daniel Avila Rojas Hugo Alberto Ayala Solares e, Rishi Babu^f, Ernesto Belmont-Moreno^a, Chad Brisboisⁿ, Karen S. Caballero-Mora^b, Tomás Capistrán ^g, Alberto Carramiñana ^h, Sabrina Casanova ⁱ, Oscar Chaparro-Amaro ^j, Umberto Cotti^c, Jorge Cotzomi^k, Eduardo De la Fuente^l, Raquel Diaz Hernandez^h, Michael A. DuVernois^m, Mora Durocher^s, Juan Carlos Díaz-Vélez¹, Kristi Engelⁿ Catalina Espinoza^a, Kwok Lung Fanⁿ, Nissim Fraija^g, José Andrés García-González^o Fernando Garfias ^g, María Magdalena González ^g, Jordan A. Goodman ⁿ, J. Patrick Harding ^s, Sergio Hernandez^a, Dezhi Huang^f, Filiberto Hueyotl-Zahuantitla^b, Thomas Brian Humenskyⁿ, Petra Hüntemeyer^f, Arturo Iriarte^g, Vikas Joshi^p, Sarah Kaufmann ^q, David Kieda ^{aa}, Alejandro Lara ^{d,*}, Jason Lee ^x, Hermes León Vargas ^{a,*}, James T. Linnemann ^r, Anna Lia Longinotti ^g, Gilgamesh Luis-Raya ^q, Kelly Malone ^{ab}, Oscar Martinez^k, Jesús Martínez-Castro^j, John A.J. Matthews^t, Pedro Miranda-Romagnoli^u, Jorge Antonio Morales-Soto^c, Eduardo Moreno^k, Amid Nayerhodaⁱ, Lukas Nellen^v, Roberto Noriega-Papaqui u, Nicola Omodei v, Yunior Pérez Araujo g, Eucario Gonzalo Pérez-Pérez q, Chang Dong Rho ad, Daniel Rosa-González h, Edna Ruiz-Velasco^y, Humberto Salazar^k, Daniel Salazar-Gallegos^r, Andres Sandoval^{a,*}, Michael Schneiderⁿ, José Serna-Franco^a, Andrew James Smithⁿ, Youngwan Son^x, Robert Wayne Springer aa, Omar Tibolla q, Kirsten Tollefson , Ibrahim Torres h, Ramiro Torres-Escobedo^z, Rhiannon Turner^f, Fernando Ureña-Mena^h, Enrique Varela^k, Luis Villaseñor k, Xiaojie Wang f, Elijah Willox n, Hao Zhou Z, Cederik de León c

^a Instituto de Física, Universidad Nacional Autónoma de México, Circuito de la Investigación Científica, Ciudad Universitaria, Ciudad de México 04510, Mexico

b Universidad Autónoma de Chiapas, Carretera Emiliano Zapata Km. 8, Rancho San Francisco, Tuxtla Gutiérrez 29050, Mexico c Universidad Michoacana de San Nicolás de Hidalgo, Edifico C-3, Ciudad Universitaria, Morelia 58040, Mexico d Instituto de Geofísica, Universidad Nacional Autónoma de México, Ciudad Universitaria, Ciudad de México 04510, Mexico e Department of Physics, Pennsylvania State University, 104 Davey Lab, University Park, PA 16802, USA
 f Department of Physics, Michigan Technological University, 1400 Townsend Drive, Houghton, MI 49931-1295, USA
 g Instituto de Astronomía, Universidad Nacional Autónoma de México, Ciudad Universitaria, Ciudad de México 04510, Mexico h Instituto Nacional de Astrofísica, Óptica y Electrónica, Luis Enrique Erro # 1, San Andres Cholula 72840, Mexico i Institute of Nuclear Physics Polish Academy of Sciences, ul. Radzikowskiego 152, Krakow PL-31342, Poland
 j Centro de Investigación en Computación, Instituto Politécnico Nacional, Av. Juan de Dios Bátiz s/n esq. Miguel Othon de Mendizabal, Ciudad de México 07738, Mexico

^k Facultad de Ciencias Físico Matemáticas, Benemérita Universidad Autónoma de Puebla, Av. San Claudio y 18 Sur, Ciudad Universitaria, Puebla 72570, Mexico

¹Departamento de Física, Centro Universitario de Ciencias Exactas e Ingenierias, Universidad de Guadalajara, Blvd. Marcelino García Barragán No. 1451, Guadalajara 44430, Mexico

^m Department of Physics, University of Wisconsin-Madison, 222 West Washington Ave., Suite 500, Madison, WI 53707, USA
ⁿ Department of Physics, University of Maryland, College Park, MD 20742-4111, USA

```
O Tecnologico de Monterrey, Escuela de Ingeniería y Ciencias, Ave. Eugenio Garza Sada 2501, Monterrey, N.L. 64849, Mexico
<sup>p</sup> Erlangen Centre for Astroparticle Physics, Friedrich-Alexander-Universität Erlangen-Nürnberg, Erwin-Rommel-Str. 1, Erlangen, BY 91058, Germany
       <sup>q</sup> Universidad Politecnica de Pachuca, Ex-Hacienda Sta. Barbara, carretera Pachuca-Cd. Sahagun Km. 20, Pachuca, Hgo 42083, Mexico
                 <sup>r</sup> Department of Physics and Astronomy, Michigan State University, 567 Wilson Road, East Lansing, MI 48824, USA
                                  <sup>8</sup> Physics Division, Los Alamos National Laboratory, Los Alamos, NM 87545, USA
           <sup>t</sup> Dept of Physics and Astronomy, University of New Mexico, 1 University of New Mexico, Albuquerque, NM 87131-0001, USA
       <sup>u</sup> Universidad Autónoma del Estado de Hidalgo, Ciudad Universitaria Carr. Pachuca-Tulancingo, km. 4.5, Pachuca, Hgo 42184, Mexico
           <sup>v</sup> Instituto de Ciencias Nucleares, Universidad Nacional Autónoma de Mexico, Circuito Exterior S/N, Mexico City 04510, Mexico
                     w Department of Physics, Stanford University, Hansen Experimental Physics Lab, Stanford, CA 94305, USA
                     x University of Seoul, 163 Seoulsiripdae-ro, Jeonnong-dong, Dongdaemun-gu, Seoul 02504, Republic of Korea
                           <sup>y</sup> Max-Planck Institute for Nuclear Physics, Saupfercheckweg 1, Heidelberg, BW69117, Germany
  <sup>z</sup> Tsung-Dao Lee Institute & School of Physics and Astronomy, Shanghai Jiao Tong University, 800 Dongchuan Rd, Shanghai, SH 200240, China
                      <sup>a</sup> Deparment of Physics and Astronomy, University of Utah, 115 S 1400 E, Salt Lake City, UT 84112, USA
                      ab Space Science and Applications Group, Los Alamos National Laboratory, Los Alamos, NM 87545, USA
                    ac School of Environmental Studies, Cochin University of Science and Technology, Kochi, Kerala 682022, India
                                   <sup>ad</sup> Department of Physics, Sungkyunkwan University, Suwon 16419, South Korea
```

Received 29 May 2023; received in revised form 19 September 2023; accepted 22 September 2023 Available online 27 September 2023

Abstract

High-energy cosmic rays that hit the Earth can be used to study large-scale atmospheric perturbations. After a first interaction in the upper parts of the atmosphere, cosmic rays produce a shower of particles that sample it down to the detector level. The HAWC (High-Altitude Water Cherenkov) gamma-ray observatory in Central Mexico at 4,100 m elevation detects air shower particles continuously with 300 water Cherenkov detectors with an active area of 12,500 m². On January 15th, 2022, HAWC detected the passage of the pressure wave created by the explosion of the Hunga volcano in the Tonga islands, 9,000 km away, as an anomaly in the measured rate of shower particles. The HAWC measurements are used to determine the propagation speed of four pressure wave passages, and correlate the variations of the shower particle rates with the barometric pressure changes. The profile of the shower particle rate and atmospheric pressure variations for the first transit of the pressure wave at HAWC is compared to the pressure measurements at the Tonga island, near the volcanic explosion. By using the cosmic-ray propagation in the atmosphere as a probe for the pressure, it is possible to achieve very high time-resolution measurements. Moreover, the high-altitude data from HAWC allows to observe the shape of the pressure anomaly with less perturbations compared to sea level detectors. Given the particular location and the detection method of HAWC, our high-altitude data provides valuable information that contributes to fully characterize this once-in-a-century phenomenon.

© 2023 COSPAR. Published by Elsevier B.V. All rights reserved.

Keywords: Lamb wave; Cosmic rays; Hunga volcano; HAWC observatory

1. Introduction

Large area cosmic-ray detectors at high elevations are a valuable tool for studying large perturbations of the Earth's atmosphere (Alvarez et al., 2021; Arunbabu et al., 2017). The cosmic rays, predominantly protons, arrive uniformly from all directions and have their first interaction at the upper layers of the atmosphere, mainly with nitrogen, oxygen or argon nuclei at typical heights of 15 to 35 km. They initiate a cascade of secondary particles that propagates through the atmosphere at almost the speed of light, reaching the maximum number of produced secondary particles at an altitude of about 6 km (Engel et al., 2011; Kampert and Unger, 2012). Beyond this shower maximum, the number of particles diminishes as

they start to be absorbed or decay, until they reach the Earth surface. During this process, the shower particles sample a large volume of the atmosphere from the height of the first interaction point down to the ground level. Given the high flux of primary cosmic rays (AMS-2 measured 1,600 protons m⁻²s⁻¹ with energies above 10 GeV (Boschini et al., 2022; Aguilar et al., 2015)), a large cosmic-ray detector at a high elevation, near the shower maximum, can detect changes in the atmospheric mass density (caused by pressure and temperature variations) to better than one part in 6,000 in the sampled volume (Abeysekara et al., 2015). On January 15th, 2022, the Hunga volcano, in several explosive events, created atmospheric pressure waves that propagated around the globe several times (Adam, 2022; Matoza et al., 2022; Wright et al., 2022). This event is by far the largest volcanic explosion in modern times. It destroyed most of the Hunga Tonga and Hunga Ha'apai islands as well as the land bridge and the crater that had formed between them in pre-

^{*} Corresponding authors.

*E-mail addresses: alara@igeofisica.unam.mx (A. Lara), hleonvar@fisica.unam.mx (H. León Vargas), asandoval@fisica.unam.mx (A. Sandoval).

vious eruptions (Otsuka, 2022). The eruption ejected tephra and gas up to the troposphere and produced waves that propagated through the Earth, the oceans, the atmosphere, and the ionosphere (Otsuka, 2022; Lin et al., 2022; Shinbori et al., 2022). The HAWC gamma-ray observatory (Abeysekara et al., 2018; Abeysekara et al., 2023), in continuous operation since March 2015, is situated on a plateau adjacent to an inactive stratovolcano in central Mexico at 4,100 m elevation. Because of its high altitude, HAWC is well placed to characterize the shape of the Lamb atmospheric pressure waves created during the explosion. Transit times of particles through the atmosphere take <1 ms, so we are measuring the integral mass of the atmosphere, not just the pressure at the surface, during the transit of the pressure wave. The PolarquEEEst cosmic-ray experiment also looked for this novel effect of the Lamb wave on the detected cosmic-ray rate but at sea level, not being able to find an associated signal (Abbrescia et al., 2022).

2. Overview of the HAWC gamma-ray observatory

The High Altitude Water Cherenkov (HAWC) observatory is located in the Pico de Orizaba National Park (latitude 18°59/41" N, longitude 97°18/31" W). In order to perform high-energy gamma-ray astronomy (from few hundred GeV up to few hundred TeV), it detects arriving air shower particles from the cascades initiated by primary gamma rays from space as they interact with the upper atmosphere. HAWC also registers the more numerous air shower events generated by primary cosmic rays that collide with the Earth's atmosphere. The observatory (shown in Fig. 1) consists of an array of 300 water Cherenkov detectors (WCD). Each WCD is a water tank of 7.3 m in diameter and 4.5 m in height, with a custom-made hermetic bag that contains 180,000 liters of ultra-pure water. The shower particles: electrons, positrons, pions, muons, and



Fig. 1. The HAWC gamma-ray observatory on the slopes of the Sierra Negra Volcano, Puebla, Mexico, at 4,100 m elevation. Air shower particles are detected in the 300 WCDs by the Cherenkov light they emit when passing through the water. The picture also shows the detector upgrade that consists of smaller WCDs that surround the main array.

low energy gammas (which produce electrons via Compton scattering) entering the water volume at almost the speed of light produce Cherenkov light, flashes of blue light, that are detected by four very sensitive photomultiplier detectors (PMT's) anchored at the bottom of each of tank (see Fig. 2). The central one is a high quantum efficiency 10-inch Hamamatsu R7081-02 PMT. Three 8-inch Hamamatsu R5912 PMTs are placed on the vertices of an equilateral triangle of 3.2 m sides. The array of 300 tanks spreads over 22,000 m² with an active area of 12,500 m² (Alfaro et al., 2017).

Relativistic shower particles that enter the water volume produce Cherenkov light, and it is enough that one photoelectron is detected by the photosensors for the data acquisition system to record the event. In this way, all signals in the photomultipliers are digitized, recording their arrival time and amplitude. The data acquisition system also records the count rate of signals in each PMT in time intervals of 25 ms and stores them in a file. HAWC aims to study cosmic rays and the sources of high-energy gamma rays, so the data acquisition system inspects all the arriving information and selects with an online computing farm only events from large showers. The trigger condition of HAWC corresponds to having more than 28 (out of \approx 1200) signals in coincidence in a 150 ns time window. The cosmic rays produce in HAWC a trigger rate of 25 kHz, these events are recorded to disk producing 2 TByte of data daily.

3. Observation results and discussion

The total single hit rate measured with all of the HAWC PMTs is of ≈ 32 MHz. This rate is highly dependent of amount of matter that the cosmic rays have to go through when propagating in the atmosphere, i.e. a larger than average density increases the absorption of particles and thus reduces the hit rate measured with HAWC. Therefore

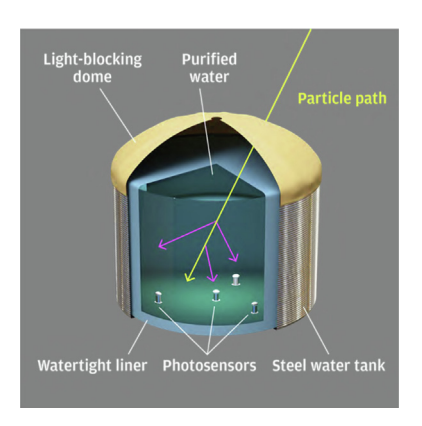


Fig. 2. Sketch of one of the 300 WCDs of the HAWC observatory. They consist of a corrugated steel cylinder of 7.3 m diameter and 4.5 m height containing a specially made airtight and lighttight bag with 180,000 liters of highly purified water. The four photosensors anchored at the bottom detect the flashes of blue light created by relativistic shower particles as they traverse the water.

HAWC is very sensitive to small changes in the properties of the atmosphere. This assumes that the cosmic-ray rate entering the atmosphere is constant in time. Although the space weather impacts this assumption, for short duration observations the detector is stable and predictable.

We performed a selection of the photomultipliers used to characterize the signal, in order to have the best accuracy in the determination of the rates. The idea was to remove those PMTs that exhibit fluctuations larger than the average for each class (8 and 10 inch) during the \approx 4-day analysis window used for this work. We performed a cut in the distribution of the standard errors calculated from the average rate of each PMT class, removing PMTs whose standard error was larger than 1σ from the mean of each class. The standard error distributions are very narrow, with long tails caused by PMTs that show large rate fluctuations during thunderstorms. A simple 1σ cut removes these problematic PMTs. In total 927 photosensors were used, 215 of the central and 712 of the peripheral PMTs.

A VAISALA PTB210 digital barometer, located inside a sea container to protect it from wind gusts, records the readings every second and it is synchronized in time with the gamma-ray detector by the same GPS signal. In this study, both the barometer data and the shower particle rates are averaged in 1-min time intervals. The dependence of the shower particle rate on variations of atmospheric conditions has been studied in the past (Alvarez et al., 2021; Arunbabu et al., 2017; De Mendonça et al., 2013; Martinelle, 1968). The results show an anti-correlation between pressure and the measured particle rate. Since the detectors are below the shower maximum, an increase in pressure increases the mass above the detector, creating greater absorption of the shower particles, which reduces the particle rate at the ground level. It is also found (De Mendonça et al., 2013; Santos et al., 2021; Savic et al., 2021) and confirmed by model calculations of the development of atmospheric showers with particle transport codes like CORSIKA, COsmic Ray SImulations for KAscade (Heck et al., 1998), that there is a linear relation between the fractional change of the particle rate to the changes in pressure:

$$\Delta R/\langle R\rangle = \alpha \Delta P + b \tag{1}$$

where the proportionality constant α is known as the barometric coefficient.

The atmospheric pressure and shower particle rate at the HAWC site show a periodic variation every 12 h because of its near-equatorial location at 19°N. These oscillations, well known for low-latitude regions, are due to atmospheric tides caused by the solar heating of the ozone and water vapor layers (Carrasco et al., 2009). The shower particle count rate shows the same oscillations but anticorrelated with the pressure variations (see Fig. 3). One can see that during the data acquisition period, from January 15 to 18th, 2022, there are short-term disturbances superimposed (with ~2 h duration) on top of these semi-

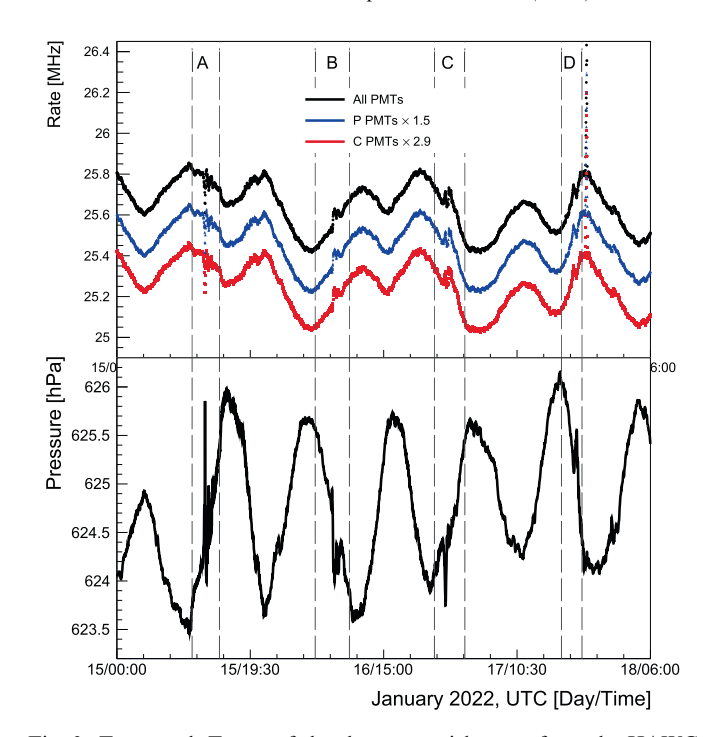


Fig. 3. Top panel: Traces of the shower particle rates from the HAWC array as a function of time from January 15th, 00:00 UTC to January 18th, 06:00 UTC. The black line shows the total rate for all considered photosensors; in blue, the subset of peripheral detectors of each tank is scaled up by a 1.5 factor; and in red, the subset of central detectors is scaled up by a 2.9 factor. The scale factors were used to display all the data with similar rate values. One sees the bi-diurnal oscillations and superimposed on them the signature of 4 passes of the Hunga explosion pressure wave, delimited by the vertical lines in regions A-D. The spike in the measured rate after the D pass is due to an electric storm at the site. Bottom panel: Pressure data from January 15th, 2022, 0:00 UTC to January 18th, 2022, 6:00 UTC. One sees the twice-daily oscillations are anti-correlated to the particle rate, and superimposed on them the pressure changes due to the passage of the pressure wave (A-D). The short path wave passages are (A) and (C), and the long path passages are (B) and (D).

diurnal variations of the particle count rate and the atmospheric pressure. These anomalies are due to the passage of the pressure wave created by the explosion of the Hunga volcano, that took place just after ~ 04:00 UTC on January 15 (Matoza et al., 2022). The count rate is shown in the top panel of Fig. 3 for the sum of all photosensors (black) and for the two independent subsets of peripheral (blue) and central (red) PMTs. One can see four passages of the pressure wave (labelled in Fig. 3 as A-D). The first (A) corresponds to the pressure wave travelling the short arm of the great circle joining Hunga with the HAWC site through the Pacific Ocean. The second (B) corresponds to the wave travelling in the opposite direction along the great circle, passing through the antipodal point in Africa and arriving at HAWC from the Atlantic side. The third (C) is the (A) wave that, after passing over HAWC, continued to the antipodal point, then to Hunga, and arrived again at the HAWC site from the Pacific direction. The fourth (D) is the (B) wave that continued to Hunga and then to the antipodal point arriving at HAWC from the Atlantic. Along the short path, the pressure wave enters through

the Mexican State of Guerrero, the highest mountains in this region are in the Oriental Volcanic Rift in Mexico with 2,200 m elevation. Along the long path, the highest elevations are on the Ethiopian High Lands, with peaks of 2,600 m elevation. The atmospheric pressure data for these days show the same four passes of the pressure wave as the shower particle rate measurements, as shown in the bottom panel of Fig. 3.

In order to extract the count rate and pressure variations due to the Hunga pressure wave, the effects of the semidiurnal oscillations must be subtracted. Since the Hunga signal for each pass extends only for 2 h, a simple procedure is applied. The short duration of the pressure anomaly is very useful to disentangle, at first order, the pressure and temperature effect on the particle count rate. The count rate and pressure variations two hours before the wave's arrival and two hours after the wave departure are fitted by a second-degree polynomial and subtracted as an average value. The fit was done with χ^2 minimization taking into account the uncertainties in the data points, which are the standard error in the mean along each axis. We also applied a more complicated procedure to characterize the background produced by the daily variations in the particle rate and pressure data, which was performed by fitting sinusoids of multiple cycles per day and found that the final barometric coefficient reported on this work changes by at most 10%. Since the pressure wave passage is a short term anomaly compared to the diurnal oscillations, the simpler approach of characterizing the semi diurnal variations with a second degree polynomial is used to conserve the fine detail features of this particular phenomenon, that are lost when using for example band-pass filters. Fig. 4 and Fig. 5 show the rate and pressure data for January 15th, 2022,

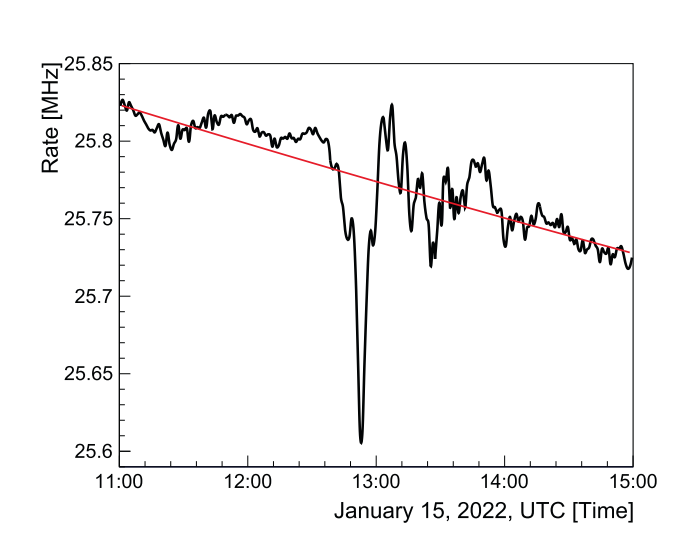


Fig. 4. Expanded view of the first pass (A) of the Hunga pressure wave as recorded by the particle rate (as measured by the sum of all PMTs) of detected shower particles from the HAWC array. A red line shows a second order polynomial fitted to the data 2 h before the wave arrival and two hours after the wave departure. The fit is used to subtract the effect of the daily oscillations on which the pressure wave signal is superimposed.

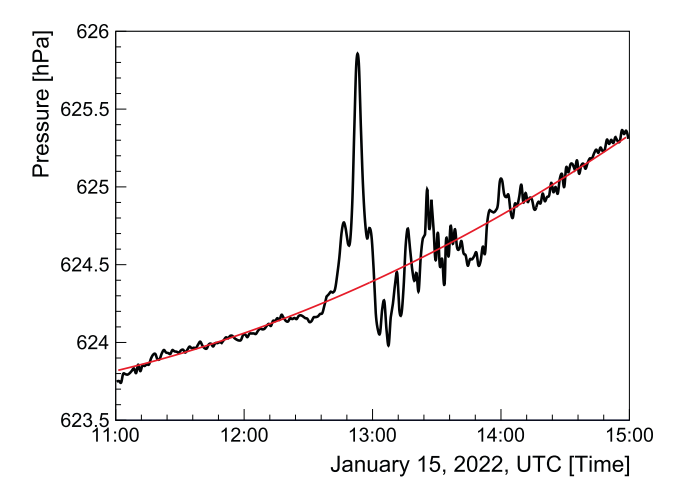


Fig. 5. Pressure data during the first pass (A) of the Hunga pressure wave from January 15th, 2022, 11:00 to 15;00 UTC, as recorded by the barometer at HAWC. A second order polynomial is fitted to the data (shown with a red line) from 2 h before the pressure wave arrival and 2 h after the wave departure. The twice-daily oscillation effect on the data is removed by subtracting the fitted polynomial function.

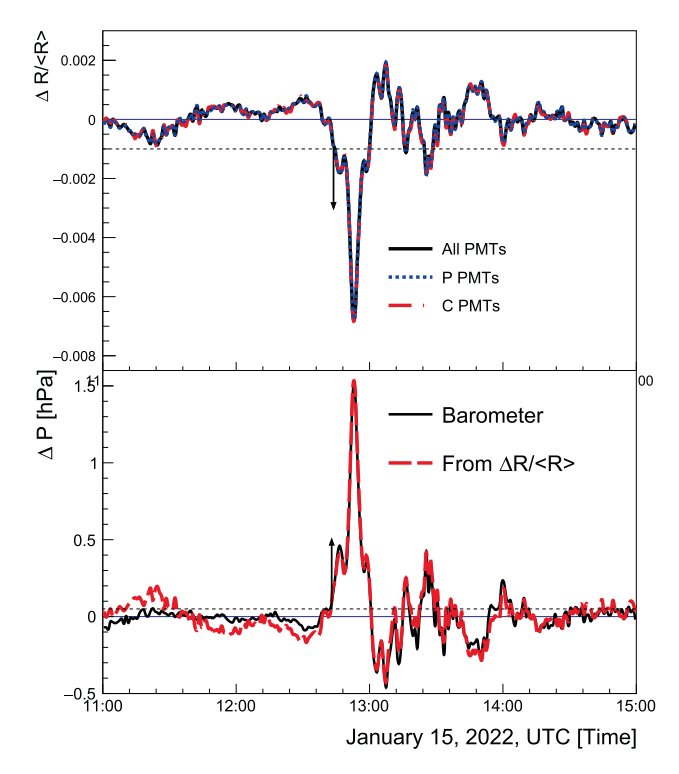


Fig. 6. Top panel: Variations on the fractional rate of detected shower particles, after the effect of the daily oscillation has been subtracted, for the time window that contains the first passage of the Hunga pressure wave. The black line shows the data for all photosensors, and the red and blue dashed lines correspond to the two independent subsets of central and peripheral sensors. The horizontal dashed line marks the fractional rate of the most significant fluctuation before the pressure wave's arrival. The point where the signal crosses this line defines the arrival time of the wave. This time is indicated by the location of the vertical arrow. Bottom panel: The black line shows the measured barometric pressure variations, with the arrival of the pressure wave indicated with the vertical arrow. The pressure variations calculated using Eq. 1, from the HAWC measured particle rate variations (top panel), are shown with the red dashed line.

from 11:00 to 15:00 UTC. The red lines gives the second-degree polynomial fit.

The top panel of Fig. 6 shows the resulting fractional change of the rate $(\Delta R/ < R >)$ for all photomultipliers as a black line, the central PMTs only with a red dashed line, and for the peripheral PMTs as the blue dashed line. The fact that the two independent subsets of sensors coincide exactly with each other shows that the procedure is robust. The bottom panel of Fig. 6 shows the atmospheric pressure variations (ΔP) as a black line, for the same time window.

It is of interest to see what is the rate-pressure correlation for the short time span during the first passage of the pressure wave. Fig. 7 shows the correlation between the measured percentile change of the shower particle rates integrated over 1 min with the instantaneous barometric pressure change for the one and a half hours after 12:40 (UTC) on January 15th 2022 during the first passage. The fitted linear correlation gives a barometric coefficient of $\alpha = -0.433 \pm 0.003$ with a correlation coefficient of -0.988. This value is consistent with a previous measurement (De Mendonça et al., 2013). We also calculated the fit just using the data points inside the main peak structure and found a consistent value for the barometric coefficient.

Utilizing this barometric coefficient one can obtain from the measured differential rate variations (top panel of Fig. 6) the associated pressure variations (red dashed curve in the bottom panel of Fig. 6). This shows that HAWC can be used as a barometer with an active area of 12,500 m², sampling the atmospheric mass density in a cone of \pm 50° above it every 25 ms.

As mentioned above, the arrival time of the pressure wave is defined as the time when the signal exceeds the most significant fluctuation seen before the arrival time of the wave. This time is indicated by arrows in both panels

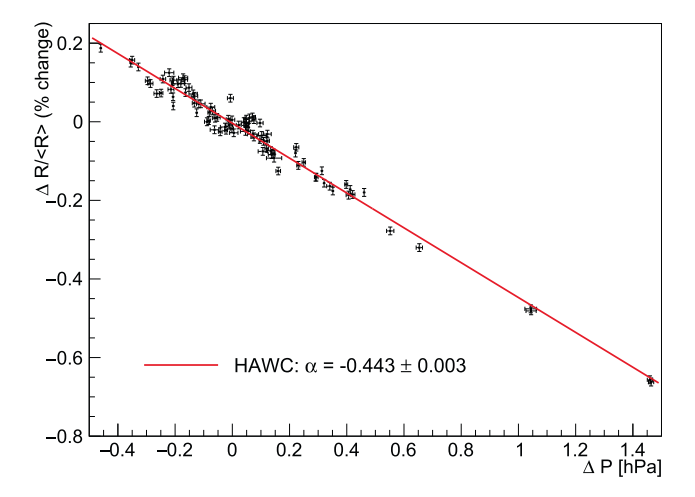


Fig. 7. Correlation diagram of the percentile rate change and the pressure variation for synchronous measurements during the passage of the first pressure wave from the Hunga explosion as recorded by the HAWC observatory in the time period from 12:40 to 14:10 UTC on January 15th, 2022. The points show the standard error on the mean for ΔP and $\Delta R/< R>.$

of Fig. 6. The same analysis was done for the other three passes of the pressure wave in order to define their arrival times. The distance along the short arc from the volcano to the HAWC observatory was calculated using the output of the IDL function MAP_2POINTS from the L3 Harris Geospatial software (Geospatial, 2022) and also using the Haversine formula (Korn and Korn, 2000). The distance along the Long arc that passes through the antipode was calculated by subtracting the short arc distance from the Earth's circumference. The arrival times, reported in Table 1, are obtained with the threshold method using the rate and pressure data obtained at the HAWC site. The uncertainties reported in Table 1 come from the difference in arrival times obtained using both data sets.

The propagation speed of the pressure wave for the four passes as determined by the shower particle rate and the pressure variations are given in Table 1. One sees that the wave that initially travelled on the short arc is slightly faster than the one travelling on the long arc. The values agree with the determination by other authors (Matoza et al., 2022; Burt, 2022; Harrison, 2022; Ramírez-Herrera et al., 2022).

There is a measurement of the barometric pressure close to the volcano on the Tonga island 64 km away, as reported by Wright et al. (2022) in the Extended Data Fig. 8. For this Tonga barometric data the effect of the daily pressure modulation was corrected by the same fitting procedure done to the HAWC pressure data. Note that for the Tonga island barometric data there is a decrease in pressure instead of an increase, measured for instance at the HAWC site. The reason is because, close to the volcano, air is being pushed up by the raising column of the ejecta, producing a decrease in the local pressure. The resulting pressure anomalies are shown in Fig. 8 with a red line and the vertical scale on the right. The same figure shows the HAWC fractional rate fluctuations for the first pass of the pressure wave. The Tonga data are shifted in time to have the main peaks coincide. In the Tonga data the authors identified four subsequent explosions, being the first one the most violent. For the first explosion both the Tonga and the HAWC data show a similar structure of a principal peak with two lower amplitude lobes on each side.

Table 1 Arrival times and propagation speed of the different passes of the pressure wave as detected by HAWC at 4,100 m elevation in central Mexico. The uncertainty in the speed propagation takes into account the two different methods to obtain the arrival time of the pressure wave as well as the difference in the propagation distance calculations when using an equatorial or polar Earth radius.

Pass	Date [UTC]	Arrival time [UTC Time]	Speed [m/s]	Type
A	Jan. 15	12:43 ± 00:01	316.2 ± 1.3	Short
В	Jan. 16	$07:25 \pm 00:01$	312.4 ± 0.2	Long
C	Jan. 16	$23:48 \pm 00:03$	316.9 ± 1.9	Short
D	Jan. 17	$19:02 \pm 00:05$	312.4 ± 0.9	Long

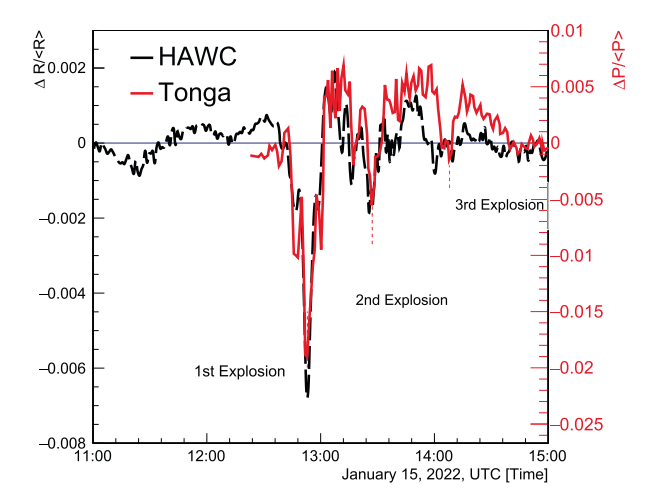


Fig. 8. Comparison of two data sets for the first pass of the pressure wave, one from the barometric pressure recorded on the Tonga island, 64 km from the Hunga eruption (red) with the vertical scale on the right, and the other from the particle rate variations detected at the HAWC site 9000 km away from Hunga (black). The pressure data from Tonga identifies three subsequent eruptions, from which the first one was the most violent. The pressure data from Tonga was shifted in time, so the most significant peaks coincide for comparison of the rate variations.

The pressure anomaly from the first pass of the pressure wave generated by the Hunga explosion shows an exponential attenuation as a function of the distance of the measurement ((Wright et al., 2022), Extended Data Fig. 1) with

$$P = 15e^{-r/2500} (2)$$

with P in hPa and r in km. The calculated amplitude at the HAWC site is 0.41 hPa, which is smaller than the observed value of 1.5 hPa, implying that the pressure wave is less attenuated at a high elevation. However, the fit quality is not very accurate at distances of 10,000 km, so it is not a solid conclusion.

The detailed study of the other transits of the Tonga pressure wave in the HAWC data is more complicated, but is in progress. The reason is that the wave's profile changes radically, and other effects, including changes in the atmosphere's temperature profile, moisture content, high electric fields or changes in the state of the heliosphere, must be evaluated. One example of such effects can be seen in Fig. 3, just after the fourth pass of the pressure wave was detected at HAWC. One can see a large increase in the detection rate at approximately 20:45 UTC on January 17, 2022. This sharp increase is correlated with increased electric field activity at the HAWC site, produced by a thunderstorm. We are in the process of investigating this effect on detail, but for the moment we point the interested reader to a recent work on this subject by the LHAASO Collaboration (Aharonian et al., 2023).

4. Conclusions

The HAWC observatory was built to study the sources of the highest energy gamma rays in our galaxy and beyond

(Albert et al., 2020). These are the most violent regions in our Universe, like remnants of supernovas, accreting black holes, or active galaxies (Albert et al., 2022). As part of the daily operations, it continuously records the rate of arrival of shower particles from all directions in the sky created by cosmic rays interacting in the upper atmosphere. Variations in the rate of arriving particles can be determined with a precision of 1 in 6,000. The very high rate of cosmic rays, combined with the large instrumented surface of HAWC, allows to achieve very high time-resolution measurements. In this paper we restricted to time bins of minutes, in order to correlate our data with a barometer, but it is possible to increase the time resolution of the HAWC data to fractions of a second.

During the January 15th–18th, 2022 period, the transits of the pressure wave created by the Hunga volcano explosion generated anomalies in the particle count rate measured by HAWC as well as pressure variations in an on site barometer. The arrival times of four passes of the wave were determined, and the resulting propagation velocities show that the portion of the Lamb wave travelling westward from Hunga is slightly faster than the part travelling to the East. The anti-correlation of the rate and pressure variations during the passage of the first arrival is linear and surprisingly tight, with a barometric coefficient α = -0.433 ± 0.003 .

The anomalies after the main event agree with the main features in the profile of the barometric pressure measurements from the Tonga island, 64 km from the volcanic eruption. They correspond to three of the four eruptions that occurred during the short period of an hour and a half. Work is in progress on a detailed analysis of the other three passages of the pressure wave created by the tremendous Hunga volcanic explosion.

The requirements needed for a ground-based gammaray observatory made possible for our detector to acquire information about the Hunga volcanic explosion in nonconventional experimental conditions. Moreover, by using cosmic rays, we are sampling the changes in the instantaneous atmospheric mass above HAWC produced by the shock wave. We expect that our measurements will be useful to the experts working on a complete characterization of this once-in-a-century phenomenon.

Declaration of competing interest

The authors declare that they have no known competing financial interests or personal relationships that could have appeared to influence the work reported in this paper.

Acknowledgments

We acknowledge the support from: the US National Science Foundation (NSF); the US Department of Energy Office of High-Energy Physics; the Laboratory Directed Research and Development (LDRD) program of Los Alamos National Laboratory; Consejo Nacional de Ciencia y Tecnología (CONACyT), México, grants CF-2023-I-645, 271051, 232656, 260378, 179588, 254964, 258865, 243290, 132197. A1-S-46288. A1-S-22784. cátedras 873. 1563. 341, 323, Red HAWC, México; DGAPA-UNAM grants IN102223, IG101320, IN111716-3, IN111419, IA102019, IN110621, IN110521; VIEP-BUAP; PIFI 2012, 2013, PROFOCIE 2014, 2015; the University of Wisconsin Alumni Research Foundation; the Institute of Geophysics, Planetary Physics, and Signatures at Los Alamos National Laboratory; Polish Science Centre grant, DEC-2017/27/B/ ST9/02272; Coordinación de la Investigación Científica de la Universidad Michoacana; Royal Society - Newton Advanced Fellowship 180385; Generalitat Valenciana, grant CIDEGENT/2018/034; The Program Management Unit for Human Resources & Institutional Development, Research and Innovation, **NXPO** (Grant B16F630069); Coordinación General Académica e Innovación (CGAI-UdeG), PRODEP-SEP UDG-CA-499; Institute of Cosmic Ray Research (ICRR), University of Tokyo. Thanks to Scott Delay, Luciano Díaz and Eduardo Murrieta for technical support.

References

- Abbrescia, M., Avanzini, C., Baldini, L., et al., 2022. Observation of Rayleigh-Lamb waves generated by the 2022 Hunga-Tonga volcanic eruption with the POLA detectors at Ny-ålesund. Sci. Rep. 12 (1), 19978. https://doi.org/10.1038/s41598-022-23984-2.
- Abeysekara, A., Albert, A., Alfaro, R., et al., 2023. The high-altitude water cherenkov (HAWC) observatory in méxico: The primary detector. Nucl. Instrum. Methods Phys. Res., Sect. A 1052, 168253. https://doi.org/10.1016/j.nima.2023.168253.
- Abeysekara, A., Alfaro, R., Alvarez, C., et al., 2018. Data acquisition architecture and online processing system for the HAWC gamma-ray observatory. Nucl. Instrum. Methods Phys. Res., Sect. A 888, 138–146. https://doi.org/10.1016/j.nima.2018.01.051.
- Abeysekara, A.U., Alfaro, R., Alvarez, C., et al., 2015. Search for gammarays from the unusually bright GRB 130427a with the HAWC gammaray observatory. Astrophys. J. 800 (2), 78. https://doi.org/10.1088/0004-637x/800/2/78.
- Adam, D., 2022. Tonga volcano eruption created puzzling ripples in earth's atmosphere. Nature 601 (497).
- Aguilar, M., Aisa, D., Alpat, B., et al.AMS Collaboration, 2015. Precision measurement of the proton flux in primary cosmic rays from rigidity 1 GV to 1.8 TV with the Alpha Magnetic Spectrometer on the international space station. Phys. Rev. Lett. 114, 171103. https://doi.org/10.1103/PhysRevLett.114.171103.
- Aharonian, F., An, Q., Axikegu, et al., 2023. Flux variations of cosmic ray air showers detected by lhaaso-km2a during a thunderstorm on june 10, 2021*. Chinese Phys. C 47 (1), 015001. https://doi.org/10.1088/1674-1137/ac9371.
- Albert, A., Alfaro, R., Alvarez, C., et al., 2020. 3hwc: The third HAWC catalog of very-high-energy gamma-ray sources. Astrophys. J. 905 (1), 76. https://doi.org/10.3847/1538-4357/abc2d8.
- Albert, A., Alfaro, R., Alvarez, C., et al., 2022. Long-term spectra of the blazars Mrk 421 and Mrk 501 at TeV energies seen by HAWC. Astrophys. J. 929 (2), 125. https://doi.org/10.3847/1538-4357/ac58f6.
- Alfaro, R., Alvarez, C., Álvarez, J., et al., 2017. All-particle cosmic ray energy spectrum measured by the HAWC experiment from 10 to 500 TeV. Phys. Rev. D 96 (12). https://doi.org/10.1103/physrevd.96.122001.
- Alvarez, C., Angeles Camacho, J.R., Arteaga-Velázquez, J.C., et al., 2021. HAWC as a ground-based space-weather observatory. Sol. Phys. 296

- (6). https://doi.org/10.1007/s11207-021-01827-z, URL: https://par.nsf.gov/biblio/10327639.
- Arunbabu, K., Ahmad, S., Chandra, A., et al., 2017. Dependence of the muon intensity on the atmospheric temperature measured by the GRAPES-3 experiment. Astropart. Phys. 94, 22–28. https://doi.org/ 10.1016/j.astropartphys.2017.07.002, URL: https://www.sciencedirect.com/science/article/pii/S0927650517300683.
- Boschini M.J., R.P., M., T., 2022. Calculator: Screened relativistic (sr) treatment for calculating the displacement damage and nuclear stopping powers for electrons, protons, light- and heavy- ions in materials (version 9.0). http://www.sr-niel.org/.
- Burt, S., 2022. Multiple airwaves crossing Britain and Ireland following the eruption of Hunga Tonga-Hunga Ha'apai on 15 January 2022. Weather, 77(3), 76–81. URL: https://rmets.onlinelibrary.wiley.com/doi/abs/10.1002/wea.4182. https://doi.org/10.1002/wea.4182. arXiv:https://rmets.onlinelibrary.wiley.com/doi/pdf/10.1002/wea.4182.
- Carrasco, E., Carramiñana, A., Avila, R., et al., 2009. Weather at sierra negra: 7.3-yr statistics and a new method to estimate the temporal fraction of cloud cover. Mon. Not. R. Astron. Soc. 398 (1), 407–421. https://doi.org/10.1111/j.1365-2966.2009.15163.x.
- De Mendonça, R.R.S., Raulin, J.P., Echer, E. et al., 2013. Analysis of atmospheric pressure and temperature effects on cosmic ray measurements. J. Geophys. Res.: Space Phys. 118(4), 1403–1409. URL: https://agupubs.onlinelibrary.wiley.com/doi/abs/10.1029/2012JA018026. https://doi.org/10.1029/2012JA018026. arXiv:https://agupubs.onlinelibrary.wiley.com/doi/pdf/10.1029/2012JA018026.
- Engel, R., Heck, D., Pierog, T., 2011. Extensive air showers and hadronic interactions at high energy. Annu. Rev. Nucl. Part. Sci. 61 (1), 467–489. https://doi.org/10.1146/annurev.nucl.012809.104544, arXiv: https://doi.org/10.1146/annurev.nucl.012809.104544.
- Geospatial, L.H., 2022. L3harris geospatial. http://www.13harrisgeospatial.com.
- Harrison, G., 2022. Pressure anomalies from the january 2022 Hunga Tonga-Hunga Ha'apai eruption. Weather, 77(3), 87–90. URL: https://rmets.onlinelibrary.wiley.com/doi/abs/10.1002/wea.4170. https://doi.org/10.1002/wea.4170. arXiv:https://rmets.onlinelibrary.wiley.com/doi/pdf/10.1002/wea.4170.
- Heck, D., Knapp, J., Capdevielle, J. et al., 1998. Corsika: a monte carlo code to simulate extensive air showers. In: Forschungszentrum Karlsruhe Report FZKA 6019.
- Kampert, K.-H., Unger, M., 2012. Measurements of the cosmic ray composition with air shower experiments. Astropart. Phys. 35 (10), 660–678. https://doi.org/10.1016/j.astropartphys.2012.02.004.
- Korn, G., Korn, T., 2000. Mathematical handbook for scientists and engineers: Definitions, theorems, and formulas for reference and review. In Dover Publications, Inc.
- Lin, J.-T., Rajesh, P.K., Lin, C.C.H. et al., 2022. Rapid conjugate appearance of the giant ionospheric lamb wave signatures in the northern hemisphere after Hunga-Tonga volcano eruptions. Geophys. Res. Lett. 49(8), e2022GL098222. URL: https://agupubs.onlinelibrary.wiley.com/doi/abs/10.1029/2022GL098222. https://doi.org/10.1029/2022GL098222. arXiv:https://agupubs.onlinelibrary.wiley.com/doi/pdf/10.1029/2022GL098222. E2022GL098222 2022GL098222.
- Martinelle, S., 1968. Air pressure dependence of cosmic ray intensity: Methods and results of a statistical analysis on neutron monitor data. Tellus, 20(1), 179–197. URL: https://onlinelibrary.wiley.com/doi/abs/10.1111/j.2153-3490.1968.tb00361.x. https://doi.org/10.1111/j.2153-3490.1968.tb00361.x. arXiv:https://onlinelibrary.wiley.com/doi/pdf/10.1111/j.2153-3490.1968.tb00361.x.
- Matoza, R.S., Fee, D., Assink, J.D. et al., 2022. Atmospheric waves and global seismoacoustic observations of the january 2022 Hunga eruption, Tonga. Science, 377(6601), 95–100. URL: https://www.science.org/doi/abs/10.1126/science.abo7063. https://doi.org/10.1126/science.abo7063. arXiv:https://www.science.org/doi/pdf/10.1126/science.abo7063.
- Otsuka, S., 2022. Visualizing lamb waves from a volcanic eruption using meteorological satellite himawari-8. Geophys. Res. Lett. 49 (8).

- https://doi.org/10.1029/2022GL098324, e2022GL098324, arXiv: https://agupubs.onlinelibrary.wiley.com/doi/pdf/10.1029/2022GL098324, E2022GL098324 2022GL098324. URL: https://agupubs.onlinelibrary.wiley.com/doi/abs/10.1029/2022GL098324.
- Ramírez-Herrera, M.T., Coca, O., Vargas-Espinosa, V., 2022. Tsunami effects on the coast of mexico by the Hunga Tonga-Hunga Ha'apai volcano eruption, Tonga. Pure Appl. Geophys. 179 (4), 1117–1137. https://doi.org/10.1007/s00024-022-03017-9.
- Santos, N.A. et al., 2021. Observations of the cosmic ray detector at the Argentine Marambio base in the Antarctic Peninsula. PoS, ICRC2021, 304. https://doi.org/10.22323/1.395.0304 (LAGO).
- Savic, M., Dragic, A., Maletic, D., et al., 2021. New empirical methods for correction of meteorological effects on cosmic ray muons. PoS, ICRC2021, 1252. https://doi.org/10.22323/1.395.1252.
- Shinbori, A., Otsuka, Y., Sori, T., et al., 2022. Electromagnetic conjugacy of ionospheric disturbances after the 2022 hunga tonga-hunga ha'apai volcanic eruption as seen in gnss-tec and superdarn hokkaido pair of radars observations. Earth, Planets Space 74 (1), 106. https://doi.org/10.1186/s40623-022-01665-8.
- Wright, C.J., Hindley, N.P., Alexander, M.J., et al., 2022. Surface-to-space atmospheric waves from Hunga Tonga-Hunga Ha'apai eruption. Nature 609 (7928), 741–746. https://doi.org/10.1038/s41586-022-05012-5.